



Consolidation of Sludge Dewatered in Geotextile Tubes under Combined Fill and Vacuum Preloading

Hao Zhang¹; Wan-jie Wang²; Si-jie Liu, Ph.D.³; Jian Chu, M.ASCE⁴; Hong-lei Sun⁵; Xue-yu Geng⁶; and Yuan-qiang Cai, M.ASCE⁷

Abstract: Recently, permeable geotextile tubes in conjunction with prefabricated horizontal drains (PHDs) have become increasingly popular for dewatering high water content slurries or sludge. However, how to analyze the consolidation process of the sludge in the geotextile tube so as to provide a proper design and prediction becomes a technical challenge. In this paper, we have proposed a two-dimensional plain-strain consolidation model for sludge consolidation in a geotextile tube under combined fill and vacuum preloading. A semi-analytical solution was obtained and validated through experimental observations. A salient finding of this study is the identification of a critical condition at which the optimum consolidation efficiency is achieved. Consolidation efficiency decreases gradually beyond this critical condition, which arrives later as the PHD pave rate and element height to width ratio increase. Furthermore, this analytical method clearly shows how preloading affects the dewatering process and the effect of fill surcharge is more pronounced than that of vacuum preloading of the same magnitude, owing to the vacuum attenuation and leakage. DOI: 10.1061/(ASCE)GT.1943-5606.0002791. © 2022 American Society of Civil Engineers.

Author keywords: Consolidation; Clay; Geotextile tube; Horizontal drain; Laboratory tests.

Introduction

With the urbanization in China, there was about 13.2 billion m³ of dredged sludge in 2019, with an expected 30% annual increase within the next ten years, resulting in land occupation and environmental pollution (Wang et al. 2019). In civil engineering applications, dredging these slurries for use as reclaimed soil, backfill, or building materials can effectively mitigate the aforementioned problems (Cheng et al. 2014; Lang et al. 2021). The disposal of these soft and highly compressible dredged materials before infrastructure can be constructed poses a variety of challenges, and many approaches to surmount it have emerged in the past few

decades (Chu et al. 2000; Miao et al. 2008; Geng et al. 2012; Rujikiatkamjorn et al. 2007; Wang et al. 2016; Cai et al. 2017, 2018, 2019). Limited by the high costs and operational complexity of conventional dewatering technologies, such as settling ponds, embankment preloads, mechanical presses, and centrifuges (Grzelak et al. 2011), the use of geotextile tubes for dewatering or the construction of geotechnical structures has garnered increasing research attention as a dewatering technique (Yee et al. 2012; Guo et al. 2013, 2015; Guo and Chu 2016; Ratnayesuraj and Bhatia 2018).

Geotextile tubes were first introduced in the 1990s to dewater municipal sewage sludge (Fowler et al. 1997), then quickly expanded to other materials, such as fly ash, coal slurry, and industrial waste (Moo-Young and Tucker 2002; Kutay and Aydilek 2004; Gulec et al. 2005; Worley et al. 2008; Yee and Lawson 2012). It aims to retain sediment and release liquid effluent through geotextile pore openings, which results in a decrease in the water content of the dewatered slurry and allows for a larger volume of slurry to be treated (Fannin et al. 1994; Leshchinsky et al. 1996; Gardoni and Palmeira 2002; Shin and Oh 2003, 2007; Yan and Chu 2010; Palmeira et al. 2011; Rowe et al. 2016). This system can be manufactured in different sizes, is easy to transport, and is simple to operate, making it an effective and viable solution for sludge dewatering, especially in high-fluidity mud (Lawson 2008; Guimarães et al. 2014; Khachan and Bhatia 2017).

However, the dewatering process of clay slurry or sludge in geotextile tubes under only its own weight is inefficient due to the extremely low permeability of the slurry or sludge (Lawson 2008; Fatema and Bhatia 2018). Therefore, prefabricated drains, which can provide extra internal drainage channels to overcome this drawback (Nagahara et al. 2004; Chai et al. 2014; Menon and Bhasi 2020), have been installed horizontally in the tubes (Guo et al. 2015). Although vertically-placed drains have been widely used in soil improvement for a long time and many theories have been developed (Geng et al. 2006, 2011; Chai et al. 2013; Zhou and Chai 2017; Spross and Larsson 2021), the combinations of

¹Ph.D. Candidate, Research Center of Coastal and Urban Geotechnical Engineering, College of Civil Engineering and Architecture, Zhejiang Univ., Hangzhou 310058, PR China. Email: h_z@zju.edu.cn

²Master's Student, College of Civil Engineering, Zhejiang Univ. of Technology, Hangzhou 310000, PR China. Email: 2111906041@zjut.edu.cn

³Postdoctoral, School of Civil Engineering, Wuhan Univ., Wuhan 430072, PR China. Email: liusijie@zju.edu.cn

⁴Professor, School of Civil and Environmental Engineering, Nanyang Technological Univ., Singapore 639798. ORCID: <https://orcid.org/0000-0003-1404-1834>. Email: cjchu@ntu.edu.sg

⁵Professor, College of Civil Engineering, Zhejiang Univ. of Technology, Hangzhou 310000, PR China (corresponding author). Email: sunhonglei@zju.edu.cn

⁶Associate Professor, School of Engineering, Univ. of Warwick, Coventry CV4 7AL, UK. Email: xueyu.geng@warwick.ac.uk

⁷Professor, Research Center of Coastal and Urban Geotechnical Engineering, College of Civil Engineering and Architecture, Zhejiang Univ., Hangzhou 310058, PR China; Professor, College of Civil Engineering, Zhejiang Univ. of Technology, Hangzhou 310000, PR China. Email: caiyq@zju.edu.cn

Note. This manuscript was submitted on September 4, 2021; approved on January 20, 2022; published online on March 22, 2022. Discussion period open until August 22, 2022; separate discussions must be submitted for individual papers. This paper is part of the *Journal of Geotechnical and Geoenvironmental Engineering*, © ASCE, ISSN 1090-0241.

vacuum-assisted prefabricated horizontal drains (PHDs) with geotextile tube systems are still in their infancy (Guo et al. 2015). However, consolidation of clay slurry or sludge in geotextile tubes under fill or vacuum surcharge is a complex process. Despite some research efforts (Leshchinsky et al. 1996; Moo-Young et al. 2002; Cantré and Saathoff 2011; Chu et al. 2011), a proper analysis and prediction that can be used for engineering design is still challenging.

In this paper, a two-dimensional plane-strain consolidation model was established to describe the dewatering process of geotextile tubes under combined surcharge and vacuum preloading. The introduction of PHDs caused the upper boundary of the unit cell to become partially drained and partially undrained. Integral transform techniques e.g., Laplace transform, Fourier cosine transform, and inverse Fourier cosine transform, were used to solve the governing, initial, and boundary equations, leading to a semi-analytical solution. The presented solution was verified by degenerating the model into a one-dimensional double-sided drainage condition and comparing the results with Terzaghi's solution and Chai and Charter's (2011) solution. Laboratory tests were also conducted to validate the proposed model. The variations in the dewatering efficiency of the geotextile tube were found to be affected by three primary variables—PHD pave rate, element height to width ratio, and the ratio of surcharge preloading to vacuum

preloading, which are discussed further to reference the engineering applications.

Analytical Model

Simplifications and Assumptions

As shown in the full-scale view of the field exercise conducted by Yee et al. (2012), the geotextile tubes laid on gravel were pumped with in-situ mud by slurry-conveying pipes [Fig. 1(a)]. After pumping, the cross-sectional shape of the geotextile tube became an ellipse. Under the combined effect of fill surcharge and vacuum preloading [Figs. 1(b and c)], water dissipated, and the tube shrank accordingly. This process was manifested mainly as vertical compression with slight lateral deformation. In laboratory tests, single circular PHD was used at the center of the geotextile tube such as reported by Guo et al. (2015). However, in practice, several rectangular PHDs could be used at a given spacing inside the geotextile tube as shown in Fig. 2(a) (Chai et al. 2014), forming a distributed drainage condition inside. In this design, H is the height of the filled geotextile tube, W is the width of the PHD, L is the spacing between the centers of adjacent PHDs, and M is the distance between the side PHD and the side of the geotextile tube.

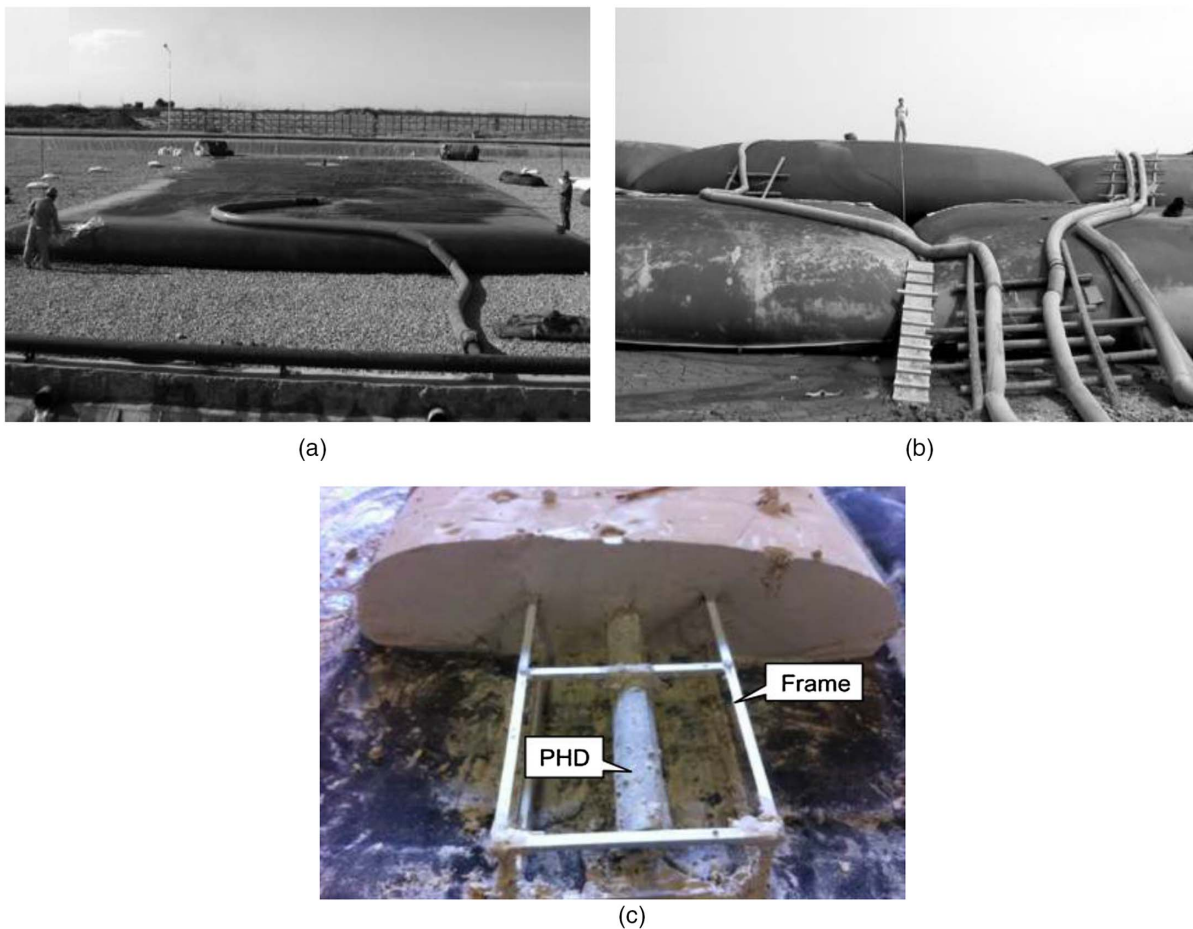


Fig. 1. Dewatering of geotextile tube: (a) self-weight dewatering; (b) dewatering under surcharge load; and (c) dewatering under vacuum pressure. [Reprinted (a and b) from *Geotextiles and Geomembranes*, Vol. 31, T. Yee, C. Lawson, Z. Wang, L. Ding, Y. Liu, “Geotextile tube dewatering of contaminated sediments, Tianjin Eco-City, China,” pp. 39–50, © 2012, with permission from Elsevier; republished (c) with permission of ICE Publishing, *Geosynthetics International*, “Model tests on methods to improve dewatering efficiency for sludge-inflated geotextile tubes,” W. Guo, J. Chu, B. Zhou, Vol. 22 (5), © 2015 permission conveyed through Copyright Clearance Center, Inc.]

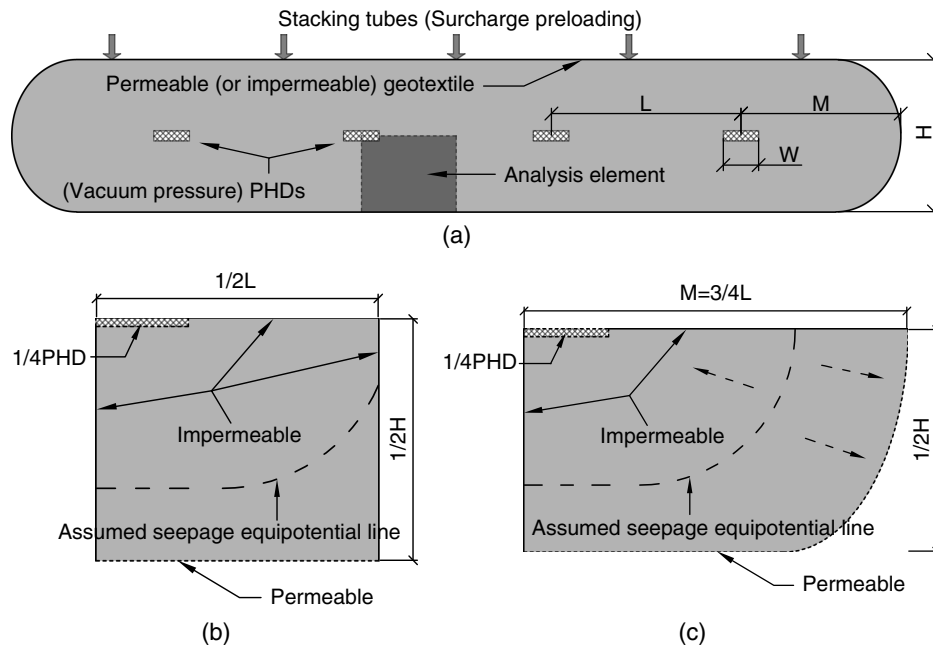


Fig. 2. Schematic model: (a) two-dimensional plane-strain model; (b) calculating unit cell; and (c) marginal unit cell.

In practical engineering applications, the stacking height of geotextile tubes could exceed 10 m [Fig. 1(b)], and the nominal vacuum pressure is -80 kPa. Considering the discharge of water from the geotextile tubes and the multiple filling of the top tube for efficiency improvements (Yee and Lawson 2012; Ratnayesuraj and Bhatia 2018), the surcharge load is assumed to be constant in this design. In addition, the average self-weight of the slurry inside the tube is included in the surcharge load. Consequently, the unit cells can be shown in Figs. 2(b and c) because of the geometric symmetry of the tube. When M is controlled to be about $3/4L$, the marginal unit cell has a larger volume and longer permeable boundary than the calculating unit cell. In this condition, comparing the seepage path and length in the calculating unit cell and the marginal unit cell, the consolidation processes of these two cells could be very similar. Therefore, the consolidation process of the entire geotextile tube could be represented by the calculating unit cell. Ignoring the thickness of the PHDs, the unit cell is divided into two sections: the PHD section and the soil section.

Governing Equation

Using the hypotheses of Terzaghi's two-dimensional consolidation theory, the governing equation of the plain-strain consolidation problem for dredged sludge dewatered in a geotextile tube can be expressed as follows:

$$\frac{\partial u}{\partial t} = C_h \frac{\partial^2 u}{\partial x^2} + C_v \frac{\partial^2 u}{\partial z^2} \quad (1)$$

where C_h and C_v are the coefficients of consolidation in the horizontal and vertical directions, respectively; u is the excess pore-water pressure; x is the horizontal coordinate; z is the vertical coordinate; and t is time.

Initial and Boundary Conditions

In this model, the time used to pump the sludge into the geotextile tube accounts for a very small proportion of the entire consolidation

duration and thus could be ignored. Thus, it is assumed that the surcharge stress, P_s , is applied to the geotextile tube instantaneously so at time zero the excess pore-water pressures at all depths in the tube increase from zero to u_s immediately, where u_s is equal to the surcharge load applied. Therefore, the initial conditions of the excess pore-water pressure in this problem can be expressed as

$$u_{t=0} = u_s = P_s \quad (2)$$

Owing to the symmetry of this model, the unit cell's lateral surfaces are considered to be impermeable. Therefore, the lateral boundary conditions can be written as follows:

$$\left. \frac{\partial u}{\partial x} \right|_{x=0} = \left. \frac{\partial u}{\partial x} \right|_{x=L/2} = 0 \quad (3)$$

This model exhibits symmetry in the vertical direction. There will be no water flow passing through the middle plane of the soil in the tube, which implies the presence of an impermeable top surface of the section without a PHD. Therefore, its boundary condition can be described as follows:

$$\left. \frac{\partial u}{\partial z} \right|_{z=0} = 0, \quad \left(\frac{W}{2} < x \leq \frac{L}{2} \right) \quad (4)$$

Because of the continuous action of vacuum pressure, P_{vac} , through the PHDs, the boundary condition of the top surface for the PHD section is

$$u|_{z=0} = u_{vac} = P_{vac}, \quad \left(0 \leq x \leq \frac{W}{2} \right) \quad (5)$$

Furthermore, to simplify the calculation, Eq. (5) is transformed into a unified form with Eq. (4) based on Darcy's law as follows:

$$\left. \frac{\partial u}{\partial z} \right|_{z=0} = -v_{PHD}(x, t) \frac{\gamma_w}{k_v}, \quad \left(0 \leq x \leq \frac{W}{2} \right) \quad (6)$$

where $v_{\text{PHD}}(x, t)$ is the drainage velocity of the PHD, k_v is the hydraulic conductivity coefficient in the vertical direction, and γ_w is the unit weight of water.

The bottom of the representative element is a permeable geotextile, so the boundary condition is

$$u|_{z=H/2} = 0 \quad (7)$$

Solutions

Normalization

To facilitate equation solving and parametric analysis, the following dimensionless parameters and variables are defined (refer to the model in Fig. 2):

1. PHD pave rate: $\alpha = W/L$, which represents the ratio between the width of the PHD, W , and the spacing of PHDs, L , which, in practice, varies between 0 and 1. When $\alpha = 1$, the PHDs will cover the entire cross-section of the tube, while $\alpha = 0$ means no PHDs;
2. Height to width ratio: $\beta = H/L$, which represents the ratio between the height of the tube, H , to the spacing of PHDs, L , and varies between 0.5 and 4 in practice;
3. Load ratio: $\Phi = P_s/|P_{\text{vac}}|$, which represents the ratio between the fill surcharge, P_s , and vacuum preloading, P_{vac} , which varies between 0.25 and 1.75 in practice;
4. Normalized excess pore-water pressure: $u_N = u/u_s$, which represents the ratio between the current excess pore-water pressure, u , and the initial pore-water pressure, u_s ;
5. Time factor: $T_v = 4C_v t/H^2$; and
6. Normalized coordinates: $X = 2x/L$ and $Z = 2z/H$.

The representative element described by the normalized parameters is given as in Fig. 3.

For a dredged slurry with high water content, the ratio of horizontal consolidation coefficient to vertical consolidation coefficient is 1. Therefore, the normalized forms of Eqs. (1), (2), (3), and (7) are as follows:

$$\frac{\partial u_N}{\partial T_v} = \beta^2 \frac{\partial^2 u_N}{\partial X^2} + \frac{\partial^2 u_N}{\partial Z^2} \quad (8)$$

$$u_N|_{T_v=0} = \Phi \quad (9)$$

$$\frac{\partial u_N}{\partial X}\bigg|_{X=0} = \frac{\partial u_N}{\partial X}\bigg|_{X=1} = 0 \quad (10)$$

$$u_N|_{Z=1} = 0 \quad (11)$$

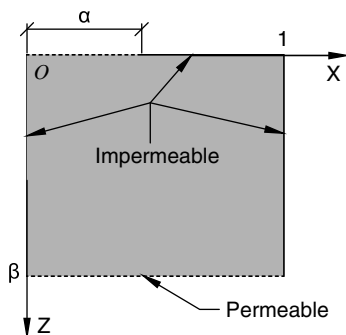


Fig. 3. Unit cell normalized.

Eqs. (4) and (6) are combined to provide a normalized equation (Chen et al. 2018) as follows:

$$\frac{\partial u_N}{\partial Z}\bigg|_{Z=0} = \begin{cases} v_N(X, T_v), & (0 \leq X \leq \alpha) \\ 0, & (\alpha < X \leq 1) \end{cases} \quad (12)$$

where $v_N(X, T_v)$ is the dimensionless drainage velocity of the PHDs, which can be expressed as

$$v_N(X, T_v) = -v_{\text{PHD}}(XL/2, T_v H^2/4C_v) \frac{\gamma_w H}{2k_v u_s} \quad (13)$$

Solutions in the Laplace Domain

The normalized consolidation model, comprising Eqs. (8)–(12), is solved using integral transform techniques such as the Laplace transform, Fourier cosine transform, and inverse Fourier cosine transform (see Appendix I for information on the detailed derivation process). The solutions for the conditions $\Phi = 0$ and $\Phi = \infty$ are listed in Appendix II. The salient solutions in the Laplace domain are presented here.

The dimensionless excess pore-water pressure in the Laplace domain is obtained as

$$\bar{u}_N(X, Z, s) = \bar{u}_{N1}(Z, s) + \bar{u}_{N2}(X, Z, s) \quad (14)$$

$$m = 0 \quad m \neq 0$$

where s is the Laplace transform variable and m is the Fourier transform variable. The term $\bar{u}_{N1}(Z, s)$ is independent of X , reflecting the average excess pore-water pressure in the X direction, while $\bar{u}_{N2}(X, Z, s)$ represents the distributed drainage effect.

The average degree of consolidation in the Laplace domain can be described as (Rujikiatkamjorn et al. 2007)

$$\bar{U}_{av}(s) = \left(\frac{\Phi - \widehat{\bar{u}_N}(s)}{\Phi - \bar{u}_\infty} \right) \times 100\% \quad (15)$$

where \bar{u}_∞ is the final average excess pore-water pressure in the Laplace domain and $\widehat{\bar{u}_N}(s)$ is the current average excess pore-water pressure in the Laplace domain for the entire soil element.

Numerical Transformation

Based on the numerical Laplace transform inversion theory proposed by Stehfest (1969), the average consolidation degree in the time domain is expressed as

$$U_{av}(T_v) = \frac{\ln 2}{T_v} \sum_{i=1}^N V(i) \bar{U} \left(\frac{\ln 2}{T_v} i \right) \quad (16)$$

where

$$V(i) = (-1)^{N/2+i} \sum_{k=\lfloor \frac{i+1}{2} \rfloor}^{\min(i, N/2)} \frac{k^{N/2} (2k)!}{(N/2 - k)! k! (k-1)! (i-k)! (2k-i)!} \quad (17)$$

And N must be a positive even integer. Theoretically, the result is more accurate as N increases. However, rounding errors worsen the result if N is too large. Stehfest (1969) suggested that the optimum N value is approximately 10 and varies for different problems. After comparing the results under different N values (Table 1), 8 was chosen to be the optimum value for this problem owing to its high accuracy and faster convergence.

Table 1. Determination of optimum N value

N	2	4	6	8	10	12	14	16	18
T_{v1}	0.0648	0.1076	0.1164	0.1173	0.1173	0.1173	0.1173	0.1173	Error
T_{v2}	0.0002	0.0021	0.0035	0.0052	0.0078	0.0111	0.0130	0.0329	Error

Note: T_{v1} = time factor corresponding to a 50% degree of consolidation; and T_{v2} = time factor corresponding to results beginning to converge. Parameters used in this determination are $\alpha = 0.2$, $\beta = 1$, $\Phi = 1$, and $\Delta t = 10$ s.



Fig. 4. Dewatering implementation process of LT1 for (a) pebbles at the bottom of the container; (b) slurry grouting; (c) PHDs laid on the surface of the geotextile tube; (d) combined vacuum and surcharge preloading; (e) end of the dewatering; and (f) profile of the final state soil.

Laboratory and Field Tests

Test Setup

Laboratory tests were carried out to verify the proposal analytical model. As shown in Fig. 4, the tests were implemented in a steel container with dimensions of 2.2 m \times 2.2 m \times 0.5 m (length \times width \times height). A layer of 0.05-m thick pebbles was spread in the container to promote bottom drainage. The geotextile tube was sewn to have a plane size of 2.0 m \times 2.0 m, with a design filling height of 0.45 m. Three and five PHDs were arranged symmetrically

in laboratory test 1 (LT1) and laboratory test 2 (LT2), respectively, and other specific parameter settings of the two laboratory tests are given in Table 2. Properties of the geotextile tube and prefabricated drain are listed in Table 3. Vacuum pumps ensured a high vacuum pressure in the water and air separation bottles, transmitting it into the tube through the PHDs. The pressure difference between the PHDs and the surrounding soils accelerated the water discharge from the PHDs and the permeable geotextile. To prevent any irregular movement of the PHDs during the dewatering process, the PHDs were fixed at the top of the steel frames inside the tube. Considering the range of variation of the tube height during consolidation, the

Table 2. Parameter settings of the laboratory and field tests

Tests	α	β	Φ	P_s (kPa)	$ P_{vac} $ (kPa)	L (m)	M (m)	H_0 (m)	w_0 (%)	w_1 (%)
LT1	0.20	0.84	0.182	5.956	32.65	0.5	0.86	0.425	180	120
LT2	0.33	1.50	0.129	7.402	57.53	0.3	0.86	0.450	180	120
FT1	0.20	1.71	0.033	1.112	80.00	0.5	0.82	0.857	245	187

Note: H_0 = initial filling height; w_0 = initial water content; w_1 = water content corresponding to the preloading applied and calculation began; P_s = surcharge preloading; and P_{vac} = vacuum pressure at the PHD.

Table 3. Properties of the geotextile and prefabricated drain

Items	Properties	Values or materials
Geotextile	Structure-polymer type	Woven multifilament polyethylene
	Thickness (mm)	1.41
	Mass density (g/m^2)	460
	Permittivity (s^{-1})	0.6
	AOS O_{90} (mm)	0.35
	Tensile strength (kN/m)	90×140
Prefabricated drain	Core plate	Co polypropylene
	Filter membrane	Non-woven fabrics
	Thickness (mm)	4.0
	Width (mm)	100
	Bending resistance	Fold in half five times
	Number of core plate ribs	30
	Longitudinal flow (cm^3/s)	≥ 40
	Tensile strength (kN/kN/10 cm)	≥ 2.0
	AOS O_{98} (μm)	80–130
	Permeability coefficient (cm/s)	0.03

Sources: Data from Hui-zhi Gao, Shandong Jianuo Engineering Materials Co., personal communication, 2021; Ya-wei Jin, Jiangsu Xintai Geotechnical Technology Co., personal communication, 2021.

PHDs were set at 0.1 m from the bottom of the tube. Further, nine miniature pore-water pressure transducers were attached to the frames to measure the pore-water pressure during dewatering. Fig. 5 shows the schematic diagrams of the testing apparatus with three PHDs.

The soil sample for LT was taken from a construction site of the Wangjiang New Town project in Shangcheng District, Hangzhou, China. Table 4 shows the basic physical and mechanical properties of the soil. The filling slurries with preset water contents, 180%, were pumped into the geotextile tube through a hose connected to the tube's upper surface by a valve. The instant average water content of the sludge in the tube is controlled by recording the sludge pumped in and water seeped out. When the sludge inside reached the designed initial average water content, 120%, the vacuum pressure and surcharge load were applied simultaneously, and the calculation was initiated. The surcharge load was applied using an impermeable bag, whose bottom dimensions were 2.2 m in length and 2.2 m in width, and filled with water for half an hour [Fig. 5(a)]. Surcharge stress is determined by the height of the water bag and ratio of the projected size of the water bag to the geotextile tube. The prefabricated drains were also laid on the extrusion surface of the water bag and the geotextile tube to ensure drainage in the tube's top surface, which can fully utilize the permeability

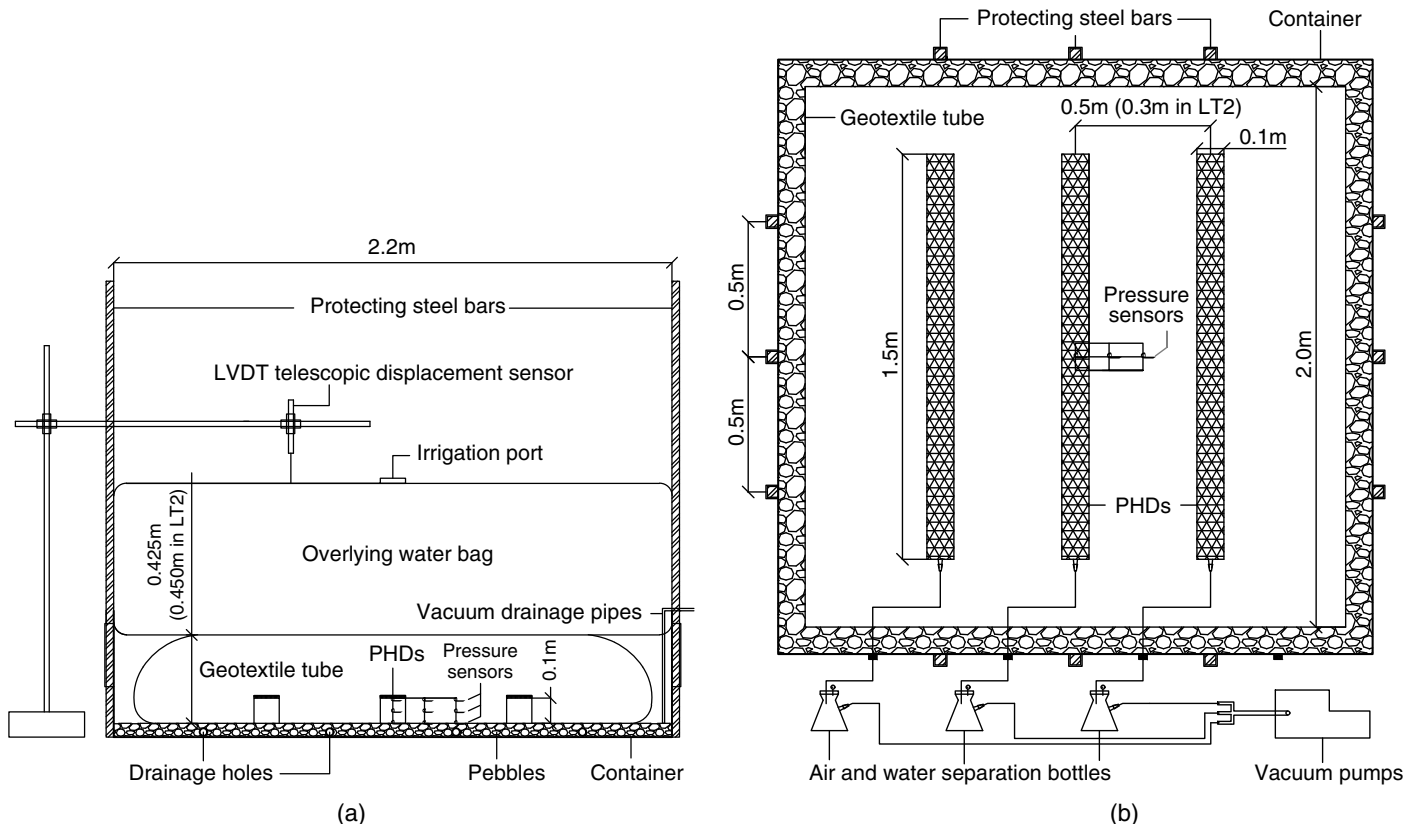


Fig. 5. Schematic diagram of LT1: (a) elevation view; and (b) commanding view.

Table 4. Soil properties

Parameters	LT1	LT2	FT1
The specific gravity of soil particles, G_s	2.67	2.67	2.53
The liquid limit, w_L (%)	26.8	26.8	39.5
The plastic limit, w_p (%)	14.1	14.1	22.0
Clay (<0.005 mm) (%)	18.8	18.8	32.5
Silt (0.005–0.075 mm) (%)	59.4	59.4	56.1
Sand (0.075–0.25 mm) (%)	21.8	21.8	11.4
Compressibility coefficient, a_v (kPa ⁻¹)	0.16	0.09	0.13
Consolidation coefficient, C_v (10 ⁻⁶ m ² /s)	1.56	1.75	0.11
Vertical permeability coefficient, k_v (10 ⁻⁷ m/s)	5.77	3.59	0.25

Note: The a_v , C_v , and k_v of LT1, LT2, and FT1 were tested in the laboratory under w_1 and load conditions of 0.5–16 kPa, 0.5–30 kPa, and 0.5–29 kPa, respectively. The maximum pressure values (16, 30, and 29 kPa) were determined by the final average effective stresses calculated by the proposed model according to surcharge stress P_s and vacuum pressure at PHDs P_{vac} .

of the geotextile. In addition, to prevent the lateral collapse of the water bag, twelve 2.5-m long protective steel bars were set on the four side plates of the container. During the tests, the height of the geotextile tube was measured using an LVDT telescopic displacement sensor mounted on an iron bracket. The top center point of the geotextile tube was taken as the height measuring point. After loading, the tube's height was obtained by subtracting the water bag's height from the elevation of the water bag's surface.

A field test (FT1) was also conducted to show the performance of this technique. As shown in Fig. 6(a), the slurries produced by the drilling holes were collected in the slurry pit and then pumped to the geotextile tube through the hose for dewatering treatment. Usually, the water content of the engineering slurry is relatively high, 245% in FT1, and a period of self-weight settlement is required after filling. The geotextile tube had an initial size of 5 m × 10 m, and the size changes with varying construction sites. Different from the laboratory model tests, nylon strings were used to fix the positions of the PHDs, because the steel frames inside the tube increased the labor and transportation costs, which is not convenient in engineering practices. Specifically, the PHDs tied by the nylon strings floated vertically at the preset height inside the tube due to buoyancy after slurry filling, and the spacing between PHDs was also constrained by the strings (Fig. 7). When the water content of the slurry decreased to a certain value, the PHDs moved downward with the soil particles and always remained close to half height of the geotextile tube. The initial height of the PHDs (i.e., length of the height-control strings) was designed according to the initial water content of the slurry and the tube height. In FT1, the tube height was 1.03 m, and the PHD height was set to be 0.4 m. More information about the locations of PHDs and pressure sensors can be found in Fig. 7. Before applying the vacuum load, the slurry extractor was used to extract some slurry to determine the current water content, which will be used for the following calculation.

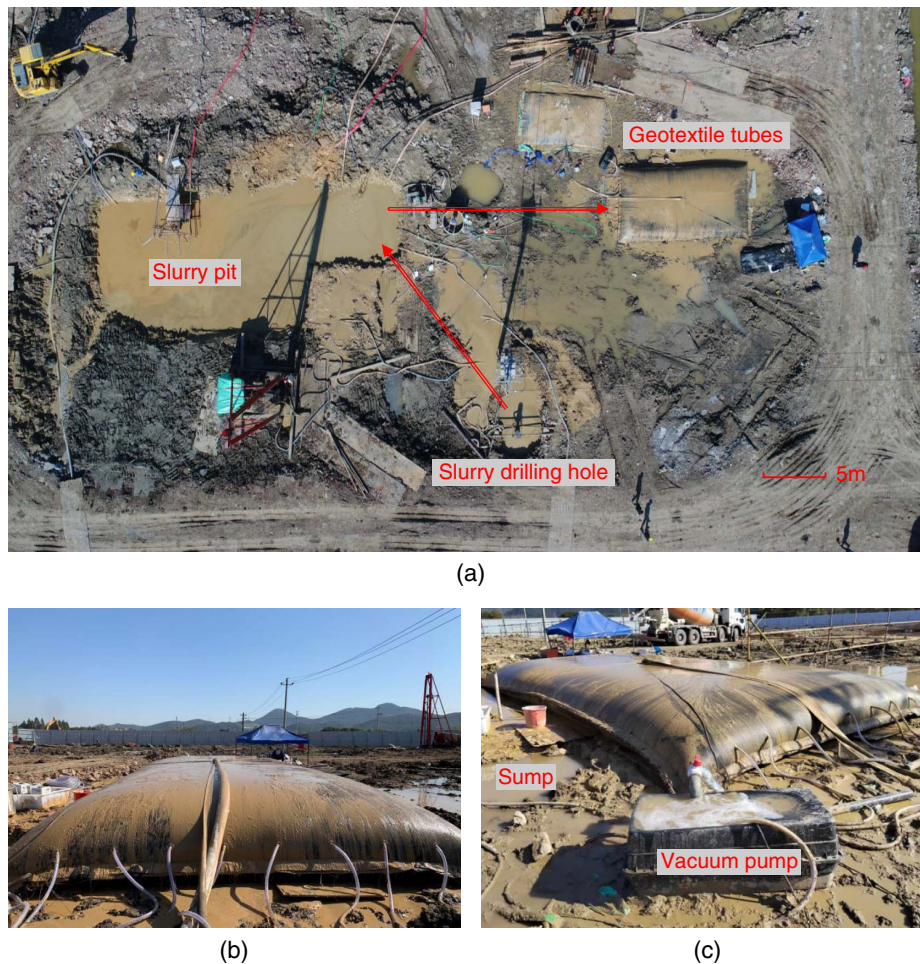


Fig. 6. Dewatering implementation process of FT1 for an (a) aerial view of the construction site; (b) initial state of the tube; and (c) geotextile tube during dewatering under vacuum preloading.

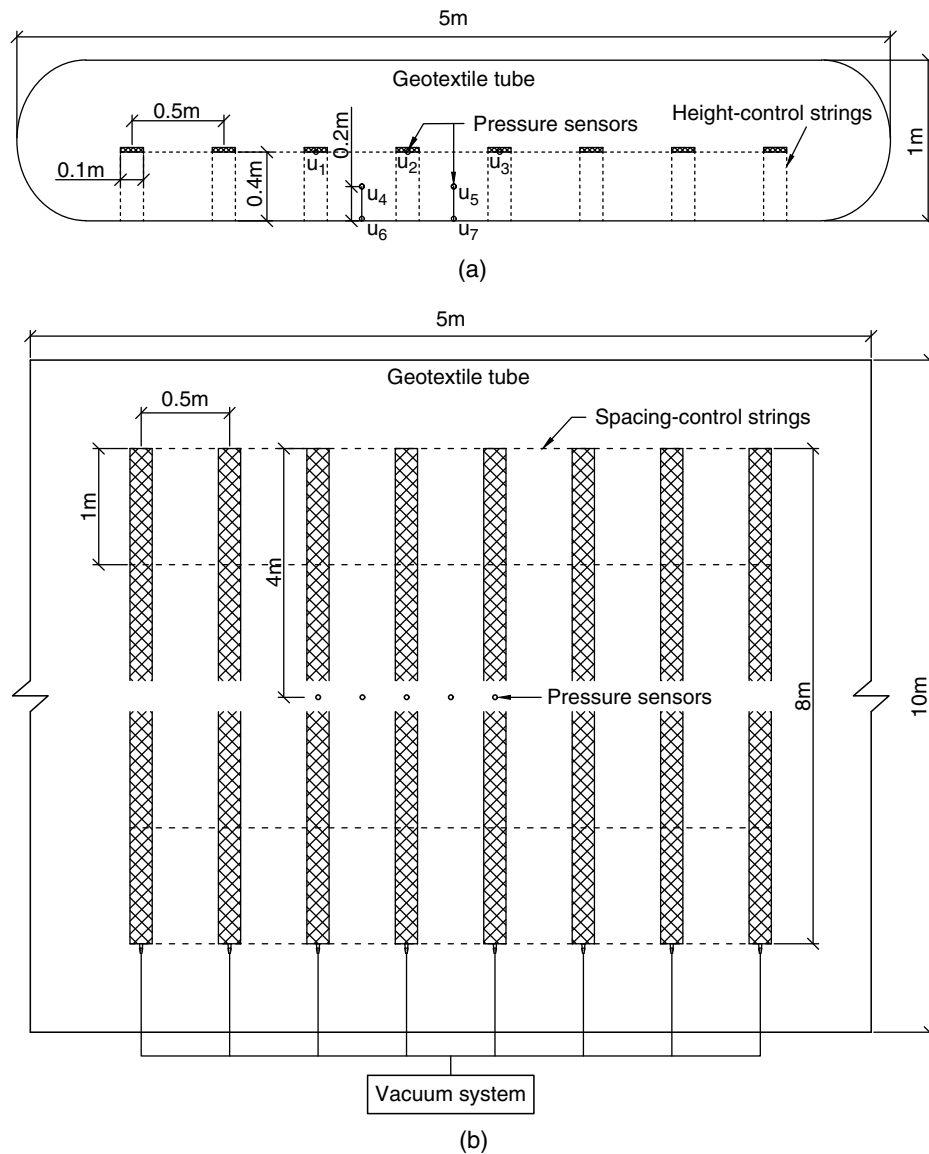


Fig. 7. Schematic diagram of FT1: (a) elevation view; and (b) commanding view.

Test Results

The experimental data are presented in Figs. 8–11, and the theoretical results obtained using the proposed model are also plotted in the same figures for comparison. The initial vertical projection sizes of the tubes in LT1 and LT2 were 1.86 m × 1.86 m, and the final vertical projection sizes were 1.90 m × 1.90 m. For FT1, the initial and recorded final vertical projection sizes are 9.36 m × 4.32 m and 9.52 m × 4.50 mm respectively. This indicated that the lateral deformation of the tube was small. Thus, the effect of lateral deformation on the height change of the tube during the tests was ignored. For LT1 and LT2, as the tube compressed, the relative height of the PHDs in the tube changed from about one-fourth to two-thirds of the tube's height. In view of the rapid change of tube height in the early consolidation stages, at about 0.1 m in half an hour, the time when the PHD deviated from the middle height of the tube was short. Therefore, on average, it was considered that the PHDs were always at the middle height of the tube during the entire process.

The calculated compressive deformation of the soil under the condition of 1D deformation is

$$S(t) = S_{\infty} U_{av}(t) \quad (18)$$

$$S_{\infty} = \frac{a_v}{1 + e_0} \sigma_{fav} H_0 \quad (19)$$

where S_{∞} is the final settlement, $S(t)$ is the settlement at time t , σ_{fav} is the final average effective stress, and $U_{av}(t)$ is the average consolidation degree at time t in the time domain.

As shown in Fig. 8, the heights of the tubes increased quickly during the filling stage. After being fully inflated, the tubes experienced a dewatering stage under the combined conditions of surcharge and vacuum preloading. The heights decreased rapidly at the beginning, stabilizing after about 9 h and 6.16 h for LT1 and LT2, respectively. Due to the small size of the geotextile tubes, the plane-strain assumption is not fully applicable, so the test results should be greater than the theoretical values during the entire process. However, in comparison to the predicted values, the measured data were slightly smaller in the later stages of consolidation. This could be caused by the unsatisfactory drainage conditions of the geotextile tube's upper surface, which squeezed against

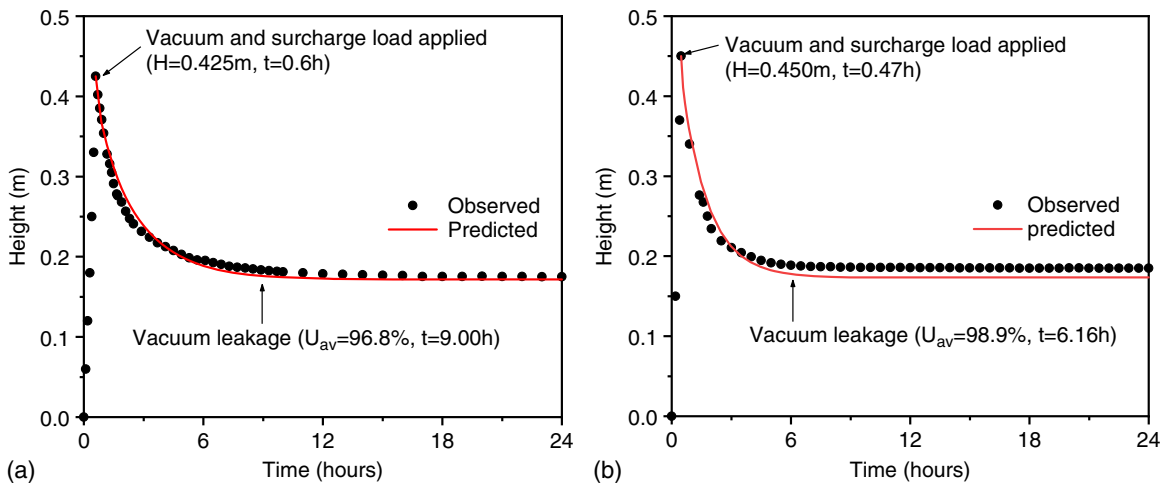


Fig. 8. Height changes of geotextile tube during dewatering for (a) LT1; and (b) LT2.

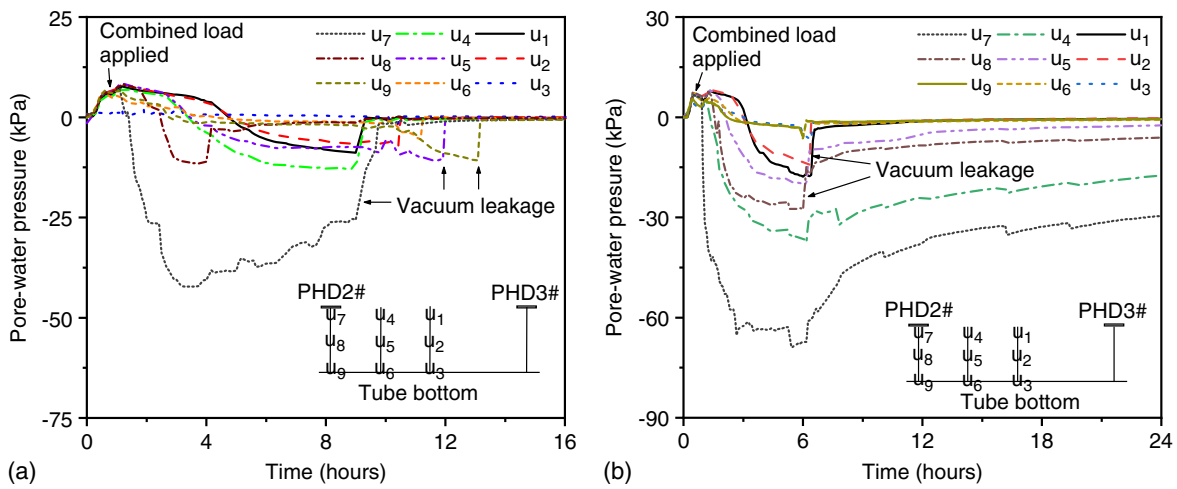


Fig. 9. Variations in pore-water pressure for (a) LT1; and (b) LT2.

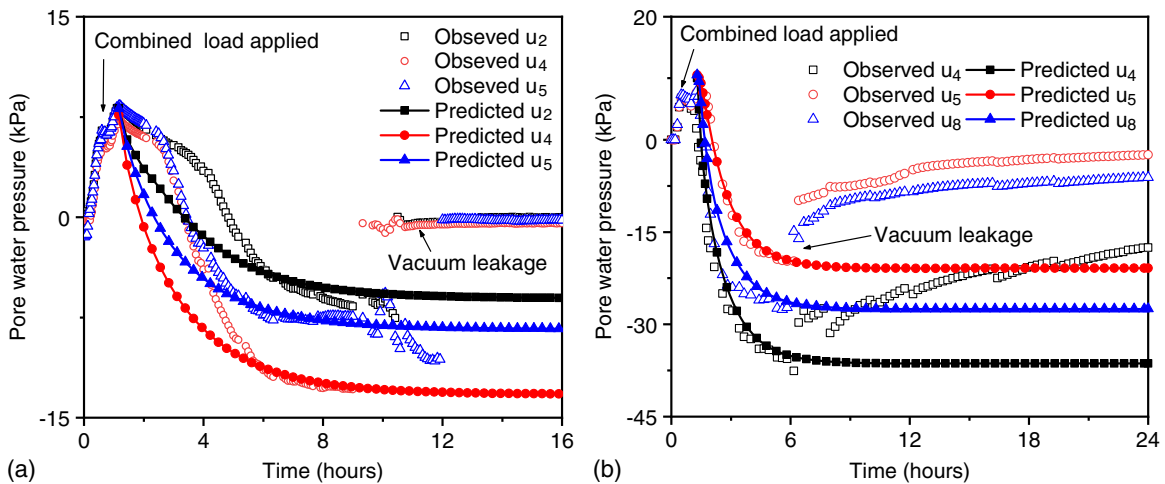


Fig. 10. Comparison of pore-water pressure between observed data and predicted values for (a) LT1; and (b) LT2.

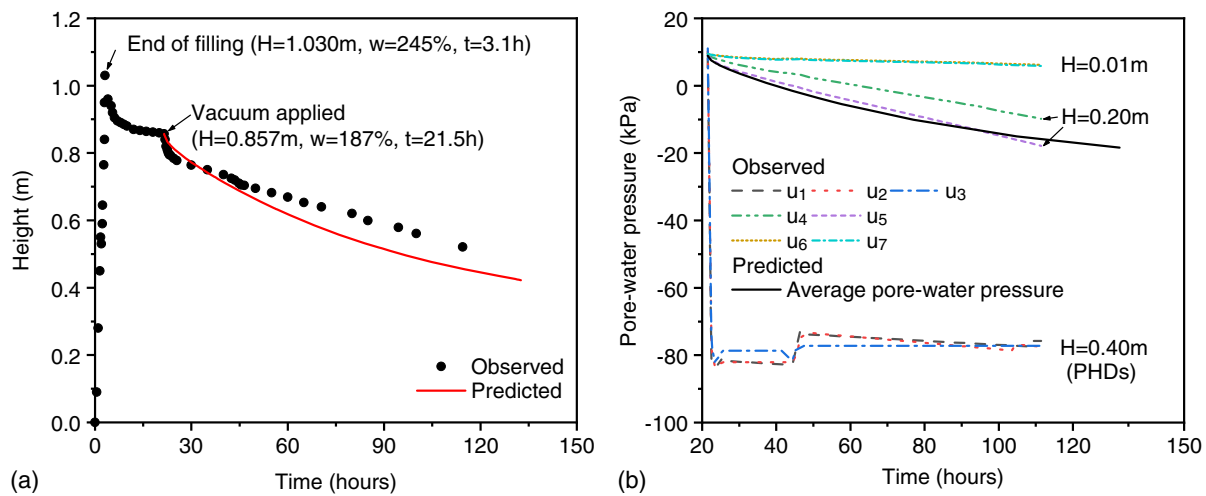


Fig. 11. Observed and predicted data for FT1: (a) variations in height; and (b) variations in pore-water pressure.

the bottom of the water bag. Further, the continuous change in the PHD's relative height during the dewatering process also affected its drainage, resulting in a smaller dehydration efficiency than the prediction. However, it can be seen from the comparative results that the influences of these factors were small. Generally speaking, the predicted height-change curves of LT1 and LT2 agreed well with the observed results.

Graphs of pore-water pressures plotted against time are presented in Fig. 9. Two peak values appeared in the variation curves, corresponding to the end of slurry filling and the end of water grouting (i.e., surcharge preloading), respectively. Subsequently, the pore-water pressures decreased when subjected to the combined preloading, and in regions closer to the PHDs, this value decreased more quickly. After a period of steady decline, sudden fluctuations began to occur. For LT1, the pore-water pressures at some measurement points suddenly changed to 0 kPa at about 9 h, while for LT2, the pore-water pressures at all measurement points changed abruptly at 6.16 h and continued to increase at a slow pace until the end of consolidation. According to the settlement results, the degree of consolidation of the two tests reached 96.8% and 98.9% in 9 h and 6.16 h, respectively, indicating that the consolidation had been completed at this moment. Therefore, the sudden change in pore-water pressure could be caused by vacuum leakage due to the formation of pore passages between the PHDs and the atmosphere when the soil dehydrates to a certain extent. The greater the external loads, the earlier this state is reached.

To validate these results, the calculated values for pore-water pressure at certain measurement points are given in Fig. 10 alongside the measured data. Pressure sensor number 7, attached to PHD, recorded the changes in the pore-water pressure at the PHD, which indicated the true pressure value applied to the geotextile tube by the vacuum pump (Fig. 9). Therefore, the value of P_{vac} used in the calculations was the average value of u_7 between the beginning of vacuum application and the time when vacuum leakage occurred. The calculated values in the figures are the sum of the theoretically calculated excess pore-water pressure and hydrostatic pressure at each pressure sensor location. It can be seen from the figures that the theoretical calculation values generally agree with the measured data before the occurrence of vacuum leakage, especially in LT2.

In field testing, the soil with finer particles was adopted, and the slurry experienced an 18.4-h self-weight dewatering process before applying the vacuum load [Fig. 11(a)]. By comparing the height changes of the geotextile tube in the self-weight dewatering stage

and the vacuum preloading stage, it is easy to conclude that PHDs can significantly improve the consolidation efficiency. However, different from the laboratory tests, the difference between the predicted height reduction value and the measured value in the field test was more prominent, about 0.09 m after 90 h. Meanwhile, FT1 showed a significant difference in pore-water pressure variation compared with LT1 and LT2. As shown in Fig. 11(b), no apparent abrupt change was found in the variation curves of pore-water pressure during the consolidation process, which indicated no vacuum leakage occurred in the geotextile tube. After 90 h of consolidation, the pore-water pressure at PHDs remained at -80 kPa, which was the nominal pressure provided by the vacuum pump. The reason for the excellent vacuum maintenance was because the consolidation was not completed at that time, which could also be concluded from the settlement curve. Pressure sensors number 4 and 5 in FT1 were fixed at a height of 20 cm from the bottom of the tube. Theoretically, their values were expected to be close to the average pore-water pressure of the entire tube in the early stage. With the development of consolidation, their relative heights increased as the height of the geotextile tube decreased, leading to a greater theoretical value than the predicted average value. However, the recorded values of pressure sensors number 4 and 5 were smaller than the predicted average value, indicating that the vacuum diffusion was not as good as expected, which also explained why the observed settlement was slower than the predicted. Therefore, the comparison of LT and FT tells that the influence of the inherent characteristics of soil on the consolidation process is decisive, such as the soil particle size distribution. Generally, the higher the clay content in the soil, the slower the dehydration and the higher the retention of vacuum pressure.

Model Performance

Evolution of Normalized Excess Pore-Water Pressure Distribution

The evolution of normalized excess pore-water pressure distribution is an intuitive phenomenon of the consolidation mechanism, revealing the specific location where consolidation develops. In this case, PHD covers 20% of the unit surface ($\alpha = 0.2$) and the height of the geotextile tube equals the spacing of the adjacent PHDs ($\beta = 1$). The surcharge load and vacuum load were 80 kPa and -80 kPa, respectively, so the load ratio Φ is 1. Figs. 12(a–d) show

the distributions of normalized excess pore-water pressure at different time factors. The maximum normalized excess pore-water pressure u_s and u_{vac} are 1 and -1 , respectively, when Φ is 1. Therefore, as a natural drainage boundary, the excess pore-water pressure at layer $Z = 1$ is always zero, while that of section $X = 0-0.2, Z = 0$ remains -1 owing to the continuous action of the vacuum pump at the PHDs. When the time factor is small, such as $T_v = 0.05$ [Fig. 12(a)], the high excess pore-water pressure caused by the surcharge preloading does not adequately dissipate, and the vacuum pressure does not effectively radiate from the PHDs. During this period, the excess pore-water pressure in the element is positive in most areas. Point $X = 1, Z = 0$ is the farthest location from the PHD and the bottom drainage boundary, resulting in it having the slowest dissipation of normalized excess pore-water pressure, a value close to 1 in the early consolidation stages. With time, the vacuum pressure diffuses, accelerating the decrease of excess pore-water pressure. The scope of negative pressure enlarges and its absolute value increases [Figs. 12(b and c)]. At the post-consolidation stage [Fig. 12(d)], nearly no positive excess pore-water pressure exists in the element, and the normalized average excess pore-water pressure for the entire analysis unit is close to the final state of -0.2844 . Furthermore, the distribution of excess pore-water pressure appears to be concentric circles centered on the PHD,

which is in accordance with the radial diffusion characteristics of vacuum pressure (Chai et al. 2010). Therefore, if $\alpha = 1$, the normalized excess pore-water pressure is consistent in the X direction and evenly decreases from -1.0 to 0 in the Z direction in the end (Chai and Charter 2011).

Final State

The final state of consolidation always corresponds to the excess pore-water pressure dissipating to zero in the traditional fully permeable consolidation model under surcharge preloading. However, when vacuum preloading is applied in conjunction with surcharge preloading, the final excess pore-water pressure in the soil becomes negative. This varies for different preloading conditions because of the attenuation characteristics of vacuum pressure along the transmission path. Therefore, in the proposed two-dimensional consolidation model with a distributed drainage boundary, the distribution of the final excess pore-water pressure is determined by the following parameters: PHD pave rate, height to width ratio, and load ratio.

As an essential factor affecting the calculation of the consolidation degree, the final average excess pore-water pressure influences the results throughout the consolidation process. Generally, the lower the final average excess pore-water pressure, the higher the final vertical effective stress, indicating a better consolidation

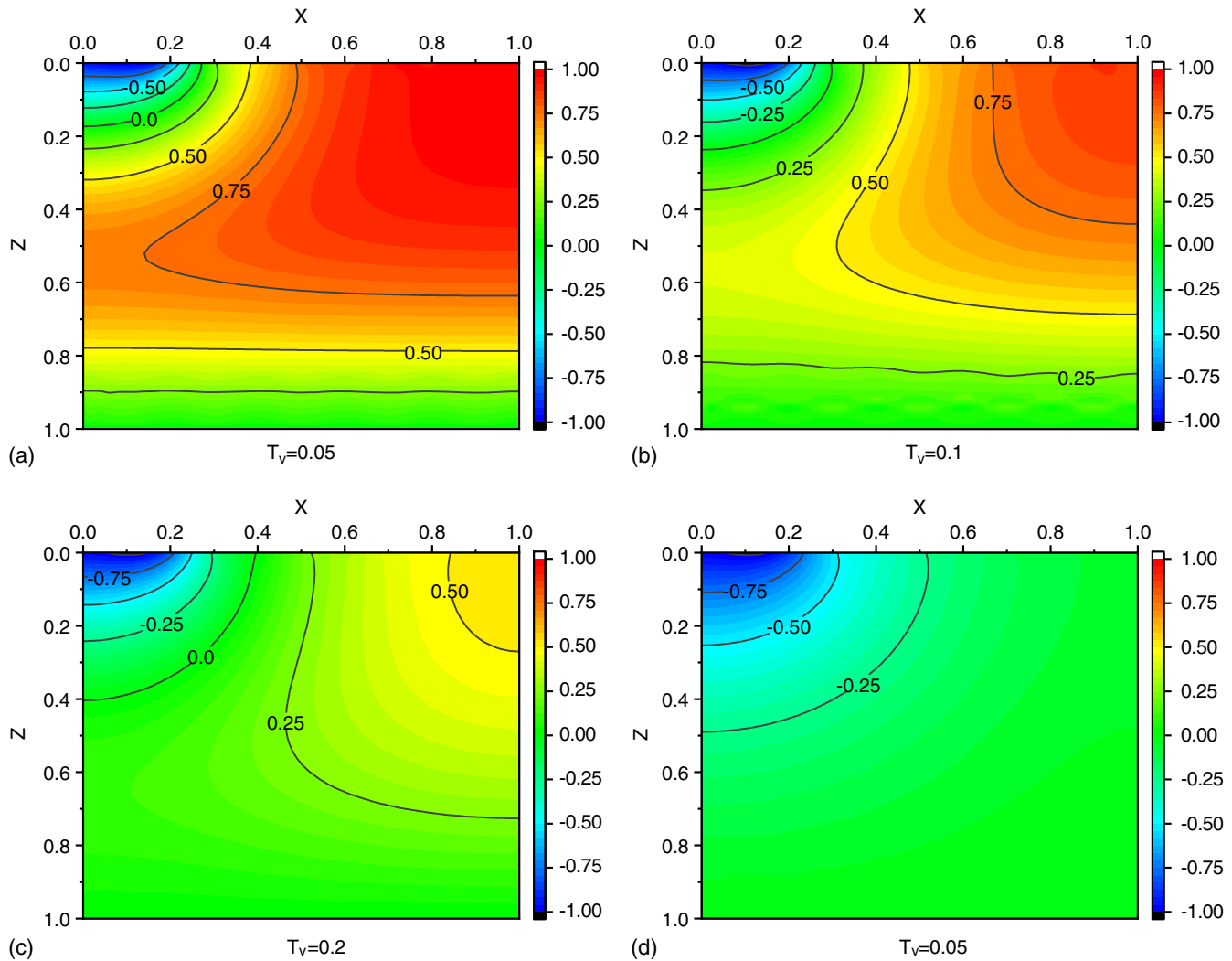


Fig. 12. Distribution of normalized excess pore-water pressure for different time factors: (a) $\alpha = 0.2, T_v = 0.05$; (b) $\alpha = 0.2, T_v = 0.1$; (c) $\alpha = 0.2, T_v = 0.2$; and (d) $\alpha = 0.2, T_v = 1$.

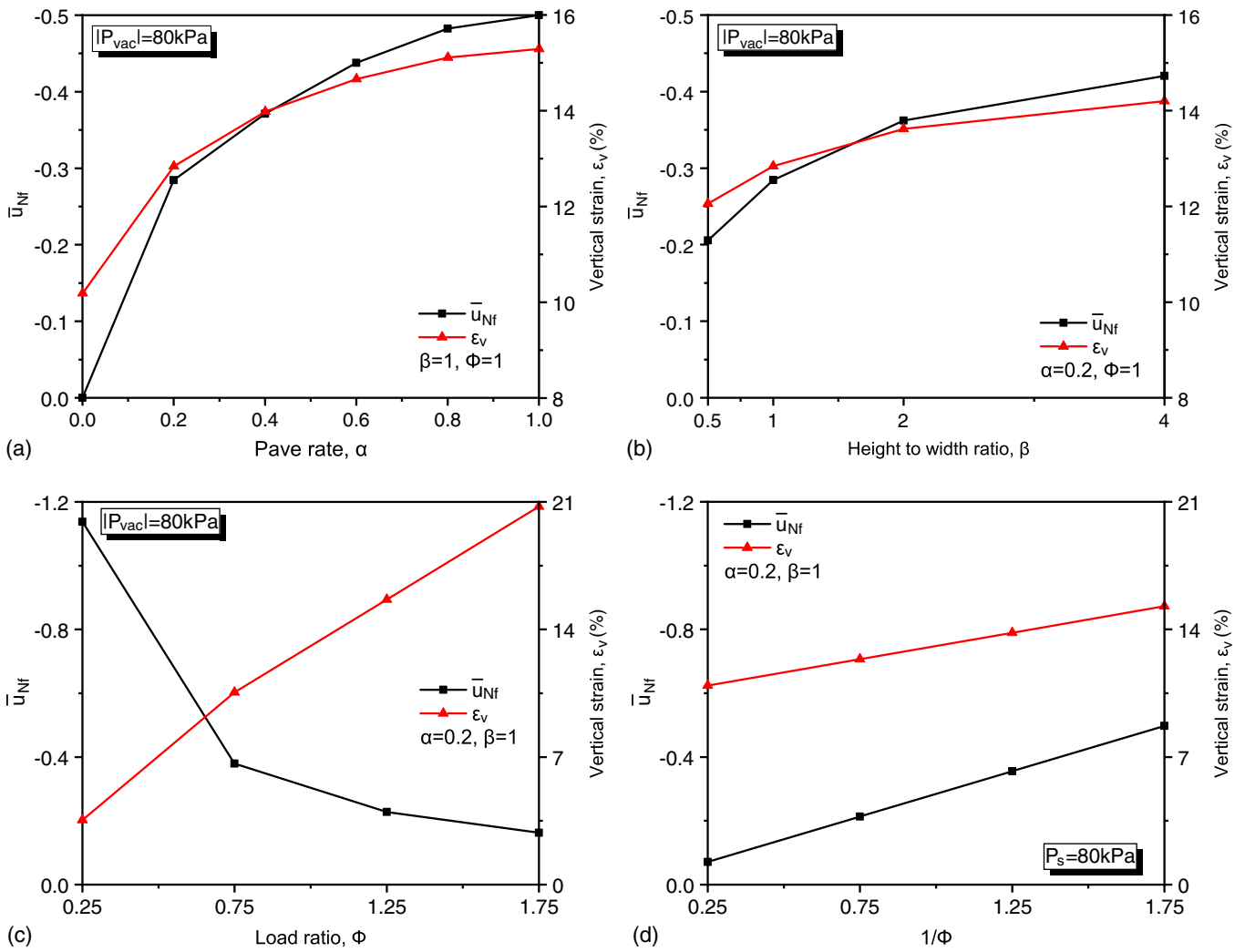


Fig. 13. Variation of the normalized final average excess pore-water pressure versus (a) PHD pave rate; (b) height to width ratio; (c) load ratio; and (d) the reciprocal of the load ratio.

effect. Figs. 13(a and b) show that the increasing PHD pave rate and height to width ratio lead to decreases in the normalized final average excess pore-water pressure \bar{u}_{Nf} to a minimum value of -0.5 , which corresponds to the fully double side drainage condition $\alpha = 1$ (Chai and Charter 2011). Obviously, the decreasing rate of \bar{u}_{Nf} slows with the increases in α and β . The vertical strain ϵ_v is an intuitive indicator of the consolidation effect, whose change law is similar to that of \bar{u}_{Nf} . It also has a maximum value of 15.3% under conditions of $H = 1$, $C_v = 4 \times 10^{-8} \text{ m}^2/\text{s}$, and $k_v = 5 \times 10^{-10} \text{ m/s}$.

Figs. 13(c and d) show the relationships between \bar{u}_{Nf} and ϵ_v versus Φ and $1/\Phi$, respectively. Φ changes with P_s under a fixed value of $|P_{vac}| = 80 \text{ kPa}$, while $1/\Phi$ varies with $|P_{vac}|$ under a fixed value of $P_s = 80 \text{ kPa}$. This clearly reveals that, with increasing Φ and $1/\Phi$, ϵ_v increases almost linearly, which is in accordance with the findings of Lu et al. (2019). Further, \bar{u}_{Nf} increases with increases in P_s [Fig. 13(c)] and decreases with increases in $|P_{vac}|$ [Fig. 13(d)]. Different values of P_s do not affect the distribution of the final excess pore-water pressure \bar{u}_f if other parameters remain constant. \bar{u}_{Nf} changes with the Φ and $1/\Phi$ values because it is defined as \bar{u}_f/u_s . Furthermore, comparing the variations of ϵ_v in the two figures, it can be concluded that for the same magnitude of surcharge preloading and vacuum preloading, the consolidation effect induced by the former is more significant than that by the

latter. In Fig. 13(d), when $1/\Phi = 1.75$, the \bar{u}_{Nf} is -0.5 and ϵ_v is 15.3%, which are equivalent to the limit case of $\alpha = 1$ in Fig. 13(a). This indicates that the additional -60 kPa vacuum pressure in this example has the same effect as the aforementioned limit condition. This comparison highlights the clear advantages of vacuum preloading in terms of the dehydration effect.

Consolidation Efficiency

To achieve the same degree of consolidation, the times required for the calculation examples under different parameters can differ, where the influence of each parameter on the model efficiency is reflected. Taking the consolidation process of no PHD paved conditions as a reference, the decreasing rate of time factor D_{T_v} was defined:

$$D_{T_v}(U_{av}, \alpha, \beta, \Phi) = \frac{T_{vz}(U_{av}) - T_{vd}(U_{av}, \alpha, \beta, \Phi)}{T_{vz}(U_{av})} \times 100\% \quad (20)$$

where T_{vd} and T_{vz} are the time factors for a certain average consolidation degree under the distributed drainage boundary condition and when $\alpha = 0$, respectively.

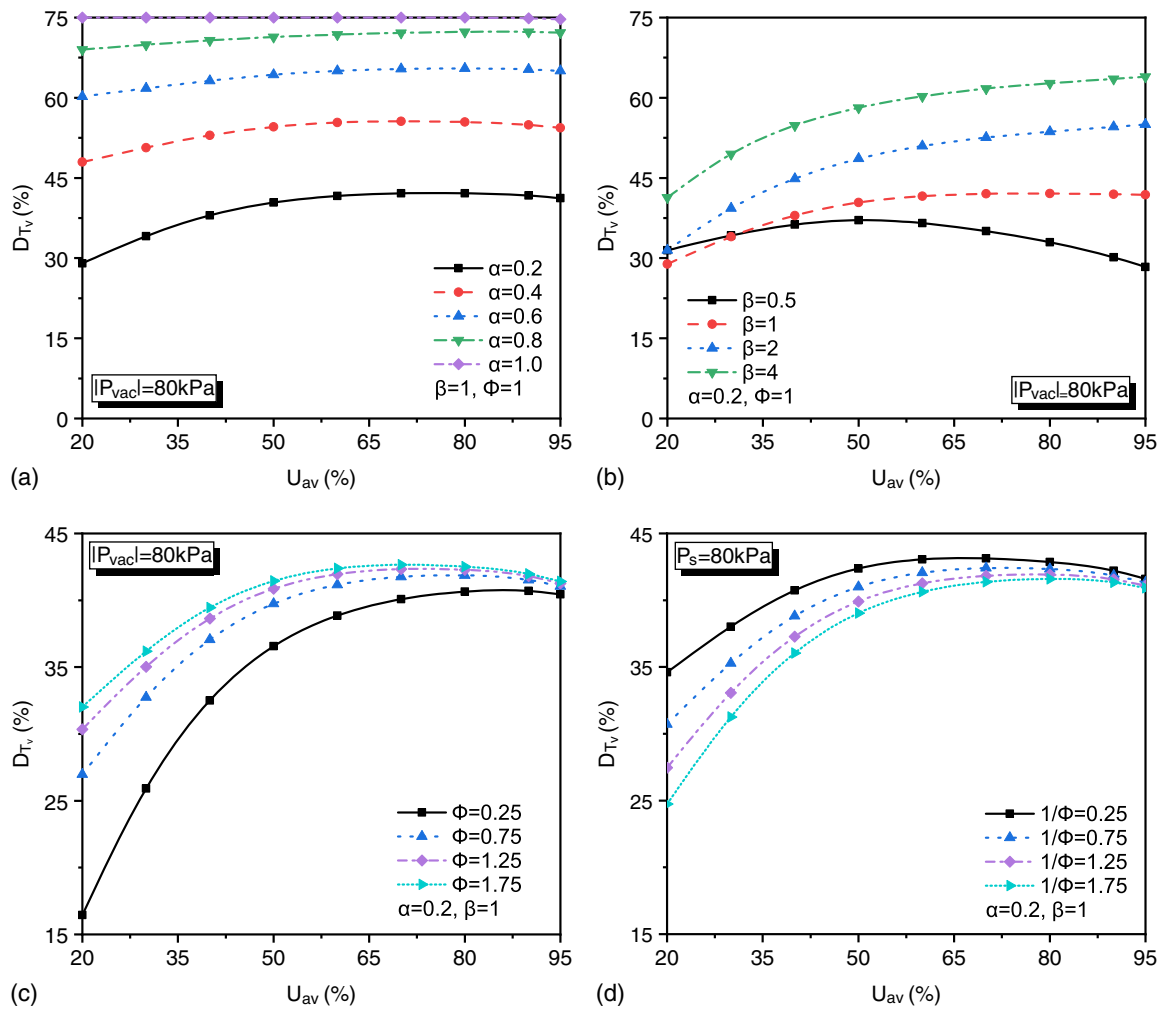


Fig. 14. Variations of the decreasing rate of time factor for different (a) PHD pave rates; (b) height to width ratios; (c) load ratios; and (d) the reciprocal of load ratios.

The relationships between the decreasing rate of time factor D_{T_v} and the parameters α , β , and Φ are plotted in Figs. 14(a-d). Generally, D_{T_v} increases with increases in α , β , and Φ . In Fig. 14(a), as consolidation develops, for curves with PHD pave rates of 20%, 40%, and 60%, a clear inflection trend can be seen, where efficiency is reduced. As the PHD pave rate continues to increase, for example, to a value of 80%, D_{T_v} increases consistently until reaching the 95% consolidation degree. The decrease in D_{T_v} signifies weakening of the PHDs' drainage promoting effect, which is influenced by the reduction in soil water yield at the later stages of consolidation. In that case, the drainage capacity of the tube system exceeds the drainage requirements of the soil inside. Although D_{T_v} always tends to zero at the end of consolidation, the greater the PHD pave rate, the later the inflection point appears. In the post stage of consolidation, the growth of D_{T_v} caused by the increase in the PHD pave rate is very limited, especially when the PHD pave rate is close to 100%. These features reveal the nonlinear relationship between D_{T_v} and α , referencing the selection of the PHD pave rate. Therefore, it is not advisable to simply increase the PHD pave rate to achieve improvements in consolidation speed.

Fig. 14(b) shows that when the height to width ratio is small (e.g., $\beta = 0.5$), the D_{T_v} value will first rise and then fall. As the height to width ratio increases, the curves will always maintain in an upward trend up to at least a consolidation degree of 95%.

The height to width ratio represents the relative size of the vertical to horizontal seepage paths. In general, the horizontal drainage path shortens with increases in height to width ratio, leading to higher consolidation efficiencies. In practical engineering, the value of β generally fluctuates around 1, considering costs and operational feasibility. Within this range, it is better to increase the value of β as much as possible to maintain a higher consolidation efficiency. The effects of different combinations of surcharge and vacuum preloading on the consolidation process are shown in Figs. 14(c and d). The evolutions of D_{T_v} for different Φ and $1/\Phi$ values have similar trajectories, first going up and then down, just like the curves in Fig. 14(b) for $\beta = 0.5$. When $|P_{vac}| = 80$ kPa, Φ increases with increases in surcharge preloading, leading to a higher consolidation rate. However, when $P_s = 80$ kPa, increasing vacuum preloading results in a reduction of D_{T_v} . In comparison to the influences of α and β , the influence of Φ on the consolidation time consumption is less significant.

Conclusions

A two-dimensional plane-strain consolidation model was established for PHD-improved geotextile tubes used for sludge dewatering under combined fill surcharge and vacuum preloading.

Using Laplace and finite Fourier cosine transformations to solve the governing equation, a semi-analytical solution was obtained. The predictions made using this solution agree well with the laboratory and field data. A series of parametric analyses on the effects of the PHD pave rate, element height to width ratio, and load ratio on the consolidation process are conducted, and the main findings are summarized as follows.

For engineering practices, the recommended values of PHD pave rate, element height to width ratio, and load ratio are 0–1, 0.5–4, and 0.25–1.75, respectively. Within these ranges, higher dewatering efficiency can be achieved by increasing these parameters.

The optimum consolidation efficiency of this tube system is found at a critical condition. After passing the critical condition, the drainage capacity of the tube system exceeds the drainage requirements of the soil inside, resulting in decreased drainage promoting effect and reduced consolidation efficiency. The larger the PHD pave rate and height to width ratio values, the later the critical condition arrives.

The contribution of surcharge load and vacuum load on consolidation development is greatly influenced by PHD pave rate and height to width ratio in this model and is directly reflected in the consolidation effect. In comparison to PHD pave rate and height to width ratio, the influence of external load on the consolidation rate is less significant, and the final dewatering effect is more evident. For surcharge preloading and vacuum preloading of the same magnitude, the consolidation of the tube system subjected to the former moves more quickly than that subjected to the latter, owing to the attenuation and leakage of vacuum pressure. Furthermore, the larger the proportion of vacuum preloading in the load combination, the slower the consolidation carries on.

The proposed solution was applied in laboratory and field tests, which verified the validity of this model. The results observed in the laboratory tests are very close to the values calculated, while the consolidation rate in the field test is slower than the theoretical prediction. In the field test, after 90 h of consolidation under –80 kPa vacuum pressure, the measured settlement is 0.301 m, while the calculated value is 0.395 m. The reasons for the difference in model and experiments may be that the drainage conditions of the surfaces of the geotextile tubes are not as ideal as the theoretical design, and the sizes of the geotextile tubes in the tests are still too small to meet the plane-strain assumption.

Appendix I. Derivation

Excess Pore-Water Pressure

According to Eq. (9), applying the Laplace transform with respect to time factor T_v , Eq. (8) can be rewritten in the following form:

$$\frac{\partial^2 \bar{u}_N}{\partial Z^2} + \beta^2 \frac{\partial^2 \bar{u}_N}{\partial X^2} - s \bar{u}_N + \Phi = 0 \quad (21)$$

The lateral boundary conditions become

$$\left. \frac{\partial \bar{u}_N}{\partial X} \right|_{X=0} = \left. \frac{\partial \bar{u}_N}{\partial X} \right|_{X=1} = 0 \quad (22)$$

The vertical boundary conditions change to

$$\left. \frac{\partial \bar{u}_N}{\partial Z} \right|_{Z=0} = \begin{cases} \bar{v}_N(X, s), & (0 \leq X \leq \alpha) \\ 0, & (\alpha < X \leq 1) \end{cases} \quad (23)$$

$$\bar{u}_N|_{Z=1} = 0 \quad (24)$$

where

$$\bar{u}_N(X, Z, s) = \int_0^\infty u_N(X, Z, T_v) e^{-sT_v} dT_v \quad (25)$$

s is the Laplace transform variable and $\bar{v}_N(X, s)$ is the dimensionless drainage velocity in the Laplace domain.

According to the lateral boundary conditions of Eq. (22), applying the finite Fourier cosine transform with respect to coordinate variable X , Eqs. (21), (23), and (24) can be expressed as:

$$\frac{\partial^2 \bar{u}_N}{\partial Z^2} - \mu_m^2 \bar{u}_N + \phi_m = 0 \quad (26)$$

$$\left. \frac{\partial \bar{u}_N}{\partial Z} \right|_{Z=0} = \int_0^\alpha \bar{v}_N(X, s) \cos(M_m X) dX \quad (27)$$

$$\bar{u}_N|_{Z=1} = 0 \quad (28)$$

where

$$\bar{u}_N(m, Z, s) = \int_0^1 \bar{u}_N(X, Z, s) \cos(M_m X) dX \quad (29)$$

$$\mu_m(s) = \sqrt{\beta^2 M_m^2 + s} \quad (30)$$

$$\phi_m = \begin{cases} \Phi, & m = 0 \\ 0, & m \neq 0 \end{cases} \quad (31)$$

and m is the Fourier transform variable, $M_m = m\pi$.

Regarding Eq. (26) as an ordinary differential equation, with respect to the boundary conditions of Eqs. (27) and (28), the solution for the excess pore-water pressure is derived as

$$\bar{u}_N(m, Z, s) = \frac{\phi_m}{\mu_m^2} \left(1 - \frac{\cosh(\mu_m Z)}{\cosh(\mu_m)} \right) + \frac{Q}{\mu_m} \left(e^{\mu_m Z} - e^{\mu_m} \frac{\cosh(\mu_m Z)}{\cosh(\mu_m)} \right) \quad (32)$$

$$Q = \int_0^\alpha \bar{v}_N(X, s) \cos(M_m X) dX \quad (33)$$

Applying the inverse finite Fourier cosine transform to Eq. (32), the dimensionless excess pore-water pressure in the Laplace domain is obtained as

$$\bar{u}_N(X, Z, s) = \bar{u}_{N1}(Z, s) + \bar{u}_{N2}(X, Z, s) \quad (34)$$

where

$$\begin{aligned} \bar{u}_{N1}(Z, s) &= \frac{\Phi}{s} \left(1 - \frac{\cosh(\mu_0 Z)}{\cosh(\mu_0)} \right) \\ &+ \frac{1}{\mu_0} \left(e^{\mu_0 Z} - e^{\mu_0} \frac{\cosh(\mu_0 Z)}{\cosh(\mu_0)} \right) \int_0^\alpha \bar{v}_N(X, s) dX, \\ (m = 0) \end{aligned} \quad (35)$$

$$\begin{aligned} \bar{u}_{N2}(X, Z, s) &= 2 \sum_{m=1}^\infty \left[\frac{\cos(M_m X)}{\mu_m} \left(e^{\mu_m Z} - e^{\mu_m} \frac{\cosh(\mu_m Z)}{\cosh(\mu_m)} \right) \right. \\ &\left. \times \int_0^\alpha \bar{v}_N(X, s) \cos(M_m X) dX \right], \quad (m \neq 0) \end{aligned} \quad (36)$$

It can be seen from Eq. (34) that the dimensionless excess pore-water pressure in the Laplace domain is determined by the value of $\overline{v_N}(X, s)$. After $\overline{v_N}(X, s)$ is obtained, the dimensionless excess pore-water pressure in the Laplace domain can be determined.

Drainage Velocity of the PHDs

The discretization method was used to obtain the solution for $\overline{v_N}(X, s)$. The PHD section can be discretized into J segments with element lengths of ΔX_j , where $\overline{v_{N-j}}(s)$ is the corresponding dimensionless drainage velocity for segment j . According to the original boundary condition of Eq. (4), for any u_N , the center of segment j should satisfy $u_N = -1$, which means that

$$\frac{\Phi}{s} \left(\frac{1}{\cosh(\mu_0)} - 1 - \frac{1}{\Phi} \right) = \sum_{j=1}^J J_{ijm}(s) \overline{v_{N-j}}(s) \quad (37)$$

where X_j is the center coordinate of the j th segment, and

$$J_{ijm}(s) = \frac{1}{\mu_0} \left(1 - \frac{e^{\mu_0}}{\cosh(\mu_0)} \right) \Delta X_j + 2 \sum_{m=1}^{\infty} \frac{1}{\mu_m} \left(1 - \frac{e^{\mu_m}}{\cosh(\mu_m)} \right) I_{mj}(X_i) \quad (38)$$

$$I_{mj}(X_i) = \frac{2}{M_m} \sin \left(M_m \frac{\Delta X_j}{2} \right) \cos(M_m X_j) \cos(M_m X_i) \quad (39)$$

Transforming Eq. (37) into a simplified form yields

$$\overline{v_{N-j}}(p) = \frac{\Phi}{s} \left(\frac{1}{\cosh(\mu_0)} - 1 - \frac{1}{\Phi} \right) \sum_{j=1}^J K_{ijm}(s) \quad (40)$$

where $K_{ijm}(s)$ is the matrix inversion of $J_{ijm}(s)$.

Average Consolidation Degree

According to Rujikiatkamjorn et al. (2007), under the conditions of combined surcharge and vacuum preloading, after the excess pore-water pressure is determined, the average consolidation degree can be conveniently expressed as follows:

$$U_c = \left(1 - \frac{\overline{u}_t}{u_s} \right) / \left(1 - \frac{\overline{u}_\infty}{u_s} \right) \times 100\% \quad (41)$$

where u_s is the surcharge load, \overline{u}_t is the mean excess pore-water pressure at time t , and \overline{u}_∞ is the final average excess pore-water pressure.

In this model, the average consolidation degree in the Laplace domain is described as

$$\overline{U}_{av}(s) = \left(\frac{\Phi - \widehat{u_N}(s)}{\Phi - \overline{u}_\infty} \right) \times 100\% \quad (42)$$

where \overline{u}_∞ is the final average excess pore-water pressure in the Laplace domain and $\widehat{u_N}(s)$ is the average excess pore-water pressure in the Laplace domain, which can be obtained by averaging $\overline{u_N}(s)$ in the X and Z directions. $\widehat{u_N}(s)$ can be expressed as

$$\widehat{u_N}(s) = \frac{\Phi}{s} \left(1 - \frac{\tanh(\mu_0)}{\mu_0} \right) + \frac{1}{\mu_0^2} (e^{\mu_0} - 1 - e^{\mu_0} \tanh(\mu_0)) \sum_{j=1}^J \overline{v_{N-j}}(s) (\Delta X_j) \quad (43)$$

Appendix II. Solutions for Single Preloading Conditions

$\Phi = 0$: Vacuum Preloading

Excess pore-water pressure:

$$\overline{u_N}(X, Z, s) = \overline{u_{N1}}(Z, s) + \overline{u_{N2}}(X, Z, s) \quad (44)$$

$$\overline{u_{N1}}(Z, s) = \frac{1}{\mu_0} \left(e^{\mu_0 Z} - e^{\mu_0} \frac{\cosh(\mu_0 Z)}{\cosh(\mu_0)} \right) \int_0^\alpha \overline{v_N}(X, s) dX, \quad (m = 0) \quad (45)$$

$$\overline{u_{N2}}(X, Z, s) = 2 \sum_{m=1}^{\infty} \left[\frac{\cos(M_m X)}{\mu_m} \left(e^{\mu_m Z} - e^{\mu_m} \frac{\cosh(\mu_m Z)}{\cosh(\mu_m)} \right) \times \int_0^\alpha \overline{v_N}(X, s) \cos(M_m X) dX \right], \quad (m \neq 0) \quad (46)$$

$$\widehat{u_N}(s) = \frac{1}{\mu_0^2} (e^{\mu_0} - 1 - e^{\mu_0} \tanh(\mu_0)) \sum_{j=1}^J \overline{v_{N-j}}(s) (\Delta X_j) \quad (47)$$

Drainage velocity of the PHD:

$$\overline{v_{N-j}}(s) = \frac{1}{s} \sum_{j=1}^J K_{ijm}(s) \quad (48)$$

$\Phi = \infty$: Surcharge Preloading

Excess pore-water pressure:

$$\overline{u_N}(X, Z, s) = \overline{u_{N1}}(Z, s) + \overline{u_{N2}}(X, Z, s) \quad (49)$$

$$\overline{u_{N1}}(Z, s) = \frac{1}{s} \left(1 - \frac{\cosh(\mu_0 Z)}{\cosh(\mu_0)} \right) + \frac{1}{\mu_0} \left(e^{\mu_0 Z} - e^{\mu_0} \frac{\cosh(\mu_0 Z)}{\cosh(\mu_0)} \right) \int_0^\alpha \overline{v_N}(X, s) dX, \quad (m = 0) \quad (50)$$

$$\overline{u_{N2}}(X, Z, s) = 2 \sum_{m=1}^{\infty} \left[\frac{\cos(M_m X)}{\mu_m} \left(e^{\mu_m Z} - e^{\mu_m} \frac{\cosh(\mu_m Z)}{\cosh(\mu_m)} \right) \times \int_0^\alpha \overline{v_N}(X, s) \cos(M_m X) dX \right], \quad (m \neq 0) \quad (51)$$

$$\widehat{u_N}(p) = \frac{1}{s} \left(1 - \frac{\tanh(\mu_0)}{\mu_0} \right) + \frac{1}{\mu_0^2} (e^{\mu_0} - 1 - e^{\mu_0} \tanh(\mu_0)) \sum_{j=1}^J \overline{v_{N-j}}(s) (\Delta X_j) \quad (52)$$

Drainage velocity of the PHD:

$$\overline{v_{N-j}}(s) = \frac{1}{s} \left(\frac{1}{\cosh(\mu_0)} - 1 \right) \sum_{j=1}^J K_{ijm}(s) \quad (53)$$

For conditions of only surcharge preloading and only vacuum preloading, $K_{ijm}(s)$ is the matrix inversion of $J_{ijm}(s)$:

$$J_{ijm}(s) = \frac{1}{\mu_0} \left(1 - \frac{e^{\mu_0}}{\cosh(\mu_0)} \right) \Delta X_j + 2 \sum_{m=1}^{\infty} \frac{1}{\mu_m} \left(1 - \frac{e^{\mu_m}}{\cosh(\mu_m)} \right) I_{mj}(X_i) \quad (54)$$

$$I_{mj}(X_i) = \frac{2}{M_m} \sin\left(M_m \frac{\Delta X_j}{2}\right) \cos(M_m X_j) \cos(M_m X_i) \quad (55)$$

Data Availability Statement

All data, models, and code generated or used during the study appear in the published article.

Acknowledgments

The work described in this paper was supported by the National Natural Science Foundation of China (Grant Nos. 52078464, 51620105008, and 51978533). The authors are very grateful for the above supports.

References

- Cai, Y. Q., H. H. Qiao, J. Wang, X. Y. Geng, P. Wang, and Y. Cai. 2017. "Experimental tests on effect of deformed prefabricated vertical drains in dredged soil on consolidation via vacuum preloading." *Eng. Geol.* 222 (May): 10–19. <https://doi.org/10.1016/j.enggeo.2017.03.020>.
- Cai, Y. Q., Z. W. Xie, J. Wang, P. Wang, and X. Y. Geng. 2018. "A new approach of vacuum preloading with booster PVDs to improve deep marine clay strata." *Can. Geotech. J.* 55 (10): 1359–1371. <https://doi.org/10.1139/cgj-2017-0412>.
- Cai, Y. Q., Z. W. Xie, J. Wang, P. Wang, and X. Y. Geng. 2019. "Reply to the discussion by mesri and kane on 'new approach of vacuum preloading with booster prefabricated vertical drains (PVDs) to improve deep marine clay strata'." *Can. Geotech. J.* 56 (12): 2017. <https://doi.org/10.1139/cgj-2019-0250>.
- Cantré, S., and F. Saathoff. 2011. "Design parameters for geosynthetic dewatering tubes derived from pressure filtration tests." *Geotext. Geomembr.* 18 (3): 90–103. <https://doi.org/10.1680/gein.2011.18.3.90>.
- Chai, J., Z. Hong, and S. Shen. 2010. "Vacuum-drain consolidation induced pressure distribution and ground deformation." *Geotext. Geomembr.* 28 (6): 525–535. <https://doi.org/10.1016/j.geotextmem.2010.01.003>.
- Chai, J. C., and J. P. Carter. 2011. *Deformation analysis in soft ground improvement*. Berlin: Springer.
- Chai, J. C., S. Horpibulsuk, S. L. Shen, and J. P. Carter. 2014. "Consolidation analysis of clayey deposits under vacuum pressure with horizontal drains." *Geotext. Geomembr.* 42 (5): 437–444. <https://doi.org/10.1016/j.geotextmem.2014.07.001>.
- Chai, J. C., C. Y. Ong, J. P. Carter, and D. T. Bergado. 2013. "Lateral displacement under combined vacuum pressure and embankment loading." *Geotechnique* 63 (10): 842–856. <https://doi.org/10.1680/geot.12.P.060>.
- Chen, Z., P. P. Ni, Y. F. Chen, and G. X. Mei. 2018. "Plane-strain consolidation theory with distributed drainage boundary." *Acta Geotech.* 15 (2): 489–508. <https://doi.org/10.1007/s11440-018-0712-z>.
- Cheng, L. S., H. Roslan, M. Shervin, and K. I. Song. 2014. "Utilization of geotextile tube for sandy and muddy coastal management: A review." *Sci. World J.* 2014 (1): 1–8. <https://doi.org/10.1155/2014/470324>.
- Chu, J., W. Guo, and S. W. Yan. 2011. "Geosynthetic tubes and geosynthetic mats: Analyses and applications." *Geotech. Eng. J.* 42 (1): 57.
- Chu, J., S. W. Yan, and H. Yang. 2000. "Soil improvement by the vacuum preloading method for an oil storage station." *Geotechnique* 50 (6): 625–632. <https://doi.org/10.1680/geot.2000.50.6.625>.
- Fannin, R. J., Y. P. Vaid, and Y. C. Shi. 1994. "Filtration behavior of non-woven geotextiles." *Can. Geotech. J.* 31 (4): 555–563. <https://doi.org/10.1139/t94-064>.
- Fatema, N., and S. K. Bhatia. 2018. "Sediment retention and clogging of geotextile with high water content slurries." *Int. J. Geosynth. Ground Eng.* 4 (2): 13. <https://doi.org/10.1007/s40891-018-0131-0>.
- Fowler, J., R. M. Bagby, and E. Trainer. 1997. "Dewatering sewage sludge with geotextile tubes." *Geotechn. Fabrics Rep.* 15 (7): 26–30.
- Gardoni, M. G., and E. M. Palmeira. 2002. "Microstructure and pore characteristics of synthetic filters under confinement." *Geotechnique* 52 (6): 405–418. <https://doi.org/10.1680/geot.2002.52.6.405>.
- Geng, X. Y., B. Indraratna, and C. Rujikiatkamjorn. 2011. "The effectiveness of partially penetrating vertical drains under a combined surcharge and vacuum preloading." *Can. Geotech. J.* 48 (6): 970–983. <https://doi.org/10.1139/t11-011>.
- Geng, X. Y., B. Indraratna, and C. Rujikiatkamjorn. 2012. "Analytical solutions for a single vertical drain with vacuum and time-dependent surcharge preloading in membrane and membraneless systems." *Int. J. Geomech.* 12 (1): 27–42. [https://doi.org/10.1061/\(ASCE\)GM.1943-5622.0000106](https://doi.org/10.1061/(ASCE)GM.1943-5622.0000106).
- Geng, X. Y., C. J. Xu, and Y. Q. Cai. 2006. "Non-linear consolidation analysis of soil with variable compressibility and permeability under cyclic loadings." *Int. J. Numer. Anal. Methods Geomech.* 30 (8): 803–821. <https://doi.org/10.1002/nag.505>.
- Grzelak, M. D., B. W. Maurer, T. S. Pullen, S. K. Bhatia, and B. V. Ramarao. 2011. "A comparison of test methods adopted for assessing geotextile tube dewatering performance." In *Proc., Geo-Frontiers 2011 Conf.*, 2141–2151. Reston, VA: ASCE.
- Guimarães, M. G. A., D. C. Urashima, and D. M. Vidal. 2014. "Dewatering of sludge from a water treatment plant in geotextile closed systems." *Geosynth. Int.* 21 (5): 310–320. <https://doi.org/10.1680/gein.14.00018>.
- Gulec, S. B., C. H. Benson, and T. B. Edil. 2005. "Effect of acidic mine drainage on the mechanical and hydraulic properties of three geosynthetics." *J. Geotech. Geoenviron. Eng.* 131 (8): 937–950. [https://doi.org/10.1061/\(ASCE\)1090-0241\(2005\)131:8\(937\)](https://doi.org/10.1061/(ASCE)1090-0241(2005)131:8(937)).
- Guo, W., and J. Chu. 2016. "Model tests and parametric studies of two-layer geomembrane tubes." *Geosynth. Int.* 23 (4): 233–246. <https://doi.org/10.1680/jgein.15.00043>.
- Guo, W., J. Chu, and S. W. Yan. 2013. "Deformation of slurry filled permeable geosynthetic tubes." In *Geo-Congress 2013: Stability and Performance of Slopes and Embankments III*, Geotechnical Special Publication 231, edited by C. Meehan, D. Pradel, M. A. Pando, and J. F. Labuz, 34–43. Reston, VA: ASCE.
- Guo, W., J. Chu, and B. Zhou. 2015. "Model tests on methods to improve dewatering efficiency for sludge-inflated geotextile tubes." *Geosynth. Int.* 22 (5): 380–392. <https://doi.org/10.1680/jgein.15.00019>.
- Khachan, M. M., and S. K. Bhatia. 2017. "The efficacy and use of small centrifuge for evaluating geotextile tube dewatering performance." *Geotext. Geomembr.* 45 (4): 280–293. <https://doi.org/10.1016/j.geotextmem.2017.04.001>.
- Kutay, M. E., and A. H. Aydilek. 2004. "Retention performance of geotextile containers confining geomaterials." *Geosynth. Int.* 11 (2): 100–113. <https://doi.org/10.1680/gein.2004.11.2.100>.
- Lang, L., B. Chen, and B. Chen. 2021. "Strength evolutions of varying water content-dredged sludge stabilized with alkali-activated ground granulated blast-furnace slag." *Constr. Build. Mater.* 275 (Mar): 122111. <https://doi.org/10.1016/j.conbuildmat.2020.122111>.
- Lawson, C. R. 2008. "Geotextile containment for hydraulic and environmental engineering." *Geosynth. Int.* 15 (6): 384–427. <https://doi.org/10.1680/gein.2008.15.6.384>.
- Leshchinsky, D., O. Leshchinsky, H. I. Ling, and P. A. Gilbert. 1996. "Geosynthetic tubes for confining pressurized slurry: Some design aspects." *J. Geotech. Eng.* 122 (8): 682–690. [https://doi.org/10.1061/\(ASCE\)0733-9410\(1996\)122:8\(682\)](https://doi.org/10.1061/(ASCE)0733-9410(1996)122:8(682)).
- Lu, Y., J. C. Chai, and W. Q. Ding. 2019. "Predicting deformation of PVD improved deposit under vacuum and surcharge loads." *Geotext. Geomembr.* 48 (1): 103502. <https://doi.org/10.1016/j.geotextmem.2019.103502>.
- Menon, A. R., and A. Bhasi. 2020. "Numerical investigation of consolidation induced by prefabricated horizontal drains (PHD) in clayey deposits." *Geotech. Geol. Eng.* 39 (3): 2101–2114. <https://doi.org/10.1007/s10706-020-01612-y>.
- Miao, L. C., X. H. Wang, and E. Kavazanjian. 2008. "Consolidation of a double-layered compressible foundation partially penetrated by deep mixed columns." *J. Geotech. Geoenviron. Eng.* 134 (8): 1210–1214. [https://doi.org/10.1061/\(ASCE\)1090-0241\(2008\)134:8\(1210\)](https://doi.org/10.1061/(ASCE)1090-0241(2008)134:8(1210)).
- Moo-Young, H. K., D. A. Gaffney, and X. Mo. 2002. "Testing procedures to assess the viability of dewatering with geotextile tubes." *Geotext.*

- Geomembr.* 20 (5): 289–303. [https://doi.org/10.1016/S0266-1144\(02\)00028-6](https://doi.org/10.1016/S0266-1144(02)00028-6).
- Moo-Young, H. K., and W. R. Tucker. 2002. “Evaluation of vacuum filtration testing for geotextile tubes.” *Geotext. Geomembr.* 20 (3): 191–212. [https://doi.org/10.1016/S0266-1144\(02\)00008-0](https://doi.org/10.1016/S0266-1144(02)00008-0).
- Nagahara, H., T. Fujiyama, T. Ishiguro, and H. Ohta. 2004. “FEM analysis of high airport embankment with horizontal drains.” *Geotext. Geomembr.* 22 (1–2): 49–62. [https://doi.org/10.1016/S0266-1144\(03\)00051-7](https://doi.org/10.1016/S0266-1144(03)00051-7).
- Palmeira, E. M., R. J. Fannin, and Y. P. Vaid. 2011. “A study on the behaviour of soil-geotextile systems in filtration tests.” *Can. Geotech. J.* 33 (6): 899–912. <https://doi.org/10.1139/t96-120>.
- Ratnayesuraj, C. R., and S. K. Bhatia. 2018. “Testing and analytical modeling of two-dimensional geotextile tube dewatering process.” *Geosynth. Int.* 25 (2): 132–149. <https://doi.org/10.1680/jgein.17.00038>.
- Rowe, R. K., P. Joshi, R. Brachman, and H. Mcleod. 2016. “Leakage through holes in geomembranes below saturated tailings.” *J. Geotech. Geoenviron. Eng.* 143 (2): 04016099. [https://doi.org/10.1061/\(ASCE\)GT.1943-5606.0001606](https://doi.org/10.1061/(ASCE)GT.1943-5606.0001606).
- Rujikiatkamjorn, C., B. Indraratna, and J. Chu. 2007. “Numerical modeling of soft soil stabilized by vertical drains, combining surcharge and vacuum preloading for a storage yard.” *Can. Geotech. J.* 44 (3): 326–342. <https://doi.org/10.1139/t06-124>.
- Shin, E. C., and Y. I. Oh. 2003. “Analysis of geotextile tube behaviour by large-scale field model tests.” *Geosynth. Int.* 10 (4): 134–141. <https://doi.org/10.1680/gein.2003.10.4.134>.
- Shin, E. C., and Y. I. Oh. 2007. “Coastal erosion prevention by geotextile tube technology.” *Geotext. Geomembr.* 25 (4–5): 264–277. <https://doi.org/10.1016/j.geotextmem.2007.02.003>.
- Spross, J., and S. Larsson. 2021. “Probabilistic observational method for design of surcharges on vertical drains.” *Géotechnique* 71 (3): 226–238. <https://doi.org/10.1680/jgeot.19.p.053>.
- Stehfest, H. 1970. “Numerical inversion of Laplace transforms.” *Commun. ACM* 13 (1): 47–49. <https://doi.org/10.1145/361953.361969>.
- Wang, H. S., C. S. Tang, K. Gu, B. Shi, and H. I. Inyang. 2019. “Mechanical behavior of fiber-reinforced, chemically stabilized dredged sludge.” *Bull. Eng. Geol. Environ.* 79 (2): 629–643. <https://doi.org/10.1007/s10064-019-01580-5>.
- Wang, J., Y. Q. Cai, J. J. Ma, J. Chu, H. T. Fu, and P. Wang. 2016. “Improved vacuum preloading method for consolidation of dredged clay-slurry fill.” *J. Geotech. Geoenviron. Eng.* 142 (11): 06016012. [https://doi.org/10.1061/\(ASCE\)GT.1943-5606.0001516](https://doi.org/10.1061/(ASCE)GT.1943-5606.0001516).
- Worley, J. W., T. M. Bass, and P. F. Vendrell. 2008. “Use of geotextile tubes with chemical amendments to dewater dairy lagoon solids.” *Bioresour. Technol.* 99 (10): 4451–4459. <https://doi.org/10.1016/j.biortech.2007.08.080>.
- Yan, S. W., and J. Chu. 2010. “Construction of an offshore dike using slurry filled geotextile mats.” *Geotext. Geomembr.* 28 (5): 422–433. <https://doi.org/10.1016/j.geotextmem.2009.12.004>.
- Yee, T. W., and C. R. Lawson. 2012. “Modelling the geotextile tube dewatering process.” *Geosynth. Int.* 19 (5): 339–353. <https://doi.org/10.1680/gein.12.00021>.
- Yee, T. W., C. R. Lawson, Z. Y. Wang, L. Ding, and Y. Liu. 2012. “Geotextile tube dewatering of contaminated sediments, Tianjin Eco-City, China.” *Geotext. Geomembr.* 31 (Apr): 39–50. <https://doi.org/10.1016/j.geotextmem.2011.07.005>.
- Zhou, Y., and J. C. Chai. 2017. “Equivalent ‘smear’ effect due to non-uniform consolidation surrounding a PVD.” *Géotechnique* 67 (5): 410–419. <https://doi.org/10.1680/jgeot.16.P.087>.